Journal of the European Ceramic Society 20 (2000) 2143–2148

Bridging stress determination by evaluation of the R-curve

T. Fett [a,*], D. Munz [a], R.D. Geraghty [b], K.W. White [b]

[a] *Forschungszentrum Karlsruhe GmbH, Institut für Materialforschung II, Postfach 3640, D-76021 Karlsruhe, Germany*
[b] *University of Houston, Department of Mechanical Engineering, Houston, TX, USA*

Received 15 November 1999; accepted 21 March 2000

Abstract

A procedure is proposed which allows for bridging stress determination from a measured R-curve. An application of the method is illustrated for a magnesium aluminate spinel ceramic that exhibits an extended linear R-curve behavior. The analytical determination of small displacement behavior and the treatment for large displacements using cubic splines is outlined in detail. After an initial increase, bridging stress values are found to decrease for larger crack opening displacements.

Keywords: Bridging stresses; $MgAl_2O_4$; R-curve

1. Introduction

Many coarse-grained ceramic materials exhibit R-curve behavior that is related to grain bridging in the wake of an advancing crack. This fact has been proved experimentally by re-notching experiments[1,2] and by in-situ observations under the electron microscope.[3,4] The observed R-curves (or K_R-curves) have often been described by a relation $K_R = f(\Delta a)$. However, it has been shown by experimental[5] and theoretical[6] investigations that the R-curve is not a unique material property. The shape of the curve depends on the geometry of the test specimens, the initial crack depth, the type of loading (tension, bending, point forces) and on the particular type of crack extension (stable and subcritical crack propagation).[7]

Although grain bridging is a very localized phenomenon, the effect has been more globally modeled in terms of bridging stresses, denoted σ_{br}. These stresses depend only on the crack face separation, δ, and when expressed in the form of $\sigma_{br} = f(\delta)$, this relationship represents a true material property, uninfluenced by test conditions. Many different experimental methods have been applied to determine the bridging stress in this form. In Refs. 8–11 bridging stresses were evaluated from the difference between crack opening profiles with and without bridging effects. A method to determine the bridging stresses from R-curves was proposed in Ref. [12] for a prescribed case of bridging in which the free parameters were ascertained. In Ref. 13 the load vs. displacement curve of controlled fracture tests was used and in Ref. 14 bridging stresses were derived from the R-curve without any assumptions on the form of the bridging function. In this case, the unknown stress distribution along the crack was modeled by a polynomial and after evaluation of the a priori unknown coefficients, the bridging stresses were obtained. The determination of a bridging function was also performed for ductile metal bridges[15] and was successfully obtained for chevron-notched specimens by Sarrafi-Nour et al.[16,17] In addition, White and Hay[18–20] successfully developed a method known as the post-fracture tensile (PFT) technique for the direct measurement of crack face interactions.

In the present investigation, a procedure will be detailed, which enables one to determine the bridging stress function from given R-curve data by a cubic spline routine. The procedure is then applied to the R-curve of a spinel microstructure.

2. Experimental results

R-curve measurements on magnesium aluminate spinel ($MgAl_2O_4$) were performed by Olasz et al.[21]. This

* Corresponding author. Tel.: +49-7247-82-4892; fax: +49-7247-82-2347.
E-mail address: theo.fett@imf.fzk.de (T. Fett).

0955-2219/00/$ - see front matter
PII: S0955-2219(00)00102-3

material has a cubic crystal structure. Therefore, no residual stresses are present in the microstructure at room temperature and a bridging zone develops solely from the grain geometry. In Fig. 1, the grain size distribution of this material is presented where the average grain size is 230 μm. Double cantilever beam (DCB) tests were performed with this material and a schematic of the specimen is shown in Fig. 2, where $H=8.5$ mm, $B=4$ mm, $L=48$ mm and $a_0=13$ mm.

The resulting R-curve is plotted in Fig. 3. This curve shows a pronounced initial straight line behavior which extends over about 6 mm crack extension due to the large grain size. We find for this range that

$$K_R = K_{I0} - K_{br}, \tag{1}$$

where the bridging stress intensity factor

$$K_{br} = C\Delta a, \quad C = -0.214\,\mathrm{MPa}\sqrt{\mathrm{m}}/\mathrm{mm} \tag{2}$$

and the stress intensity factor at the onset of crack propagation, $K_{I0}=1.45$ MPa $\sqrt{\mathrm{m}}$.

3. Basic relations

If the relationship between the bridging stress, σ_{br}, and the crack face separation, δ, is available, fracture mechanics methods enable the computation of the related R-curve. For example, Fig. 4 shows the stress distribution along the crack length of a material that exhibits a bridging zone. Here, the total stress on the crack tip is the sum of the applied stress and the bridging stress, σ_{br}, i.e.

$$\sigma(x) = \sigma_{appl}(x) + \sigma_{br}(x). \tag{3}$$

These stresses are responsible for the stress intensity factor, which is given in terms of the fracture mechanics weight function, h,[22] as

$$K_I = \int_0^a h(x/a, a/W)\,\sigma(x)\ \mathrm{d}x. \tag{4}$$

The weight function, $h(x,a)$, is a function of the crack length, a, and the coordinate, x. It depends on the geometry

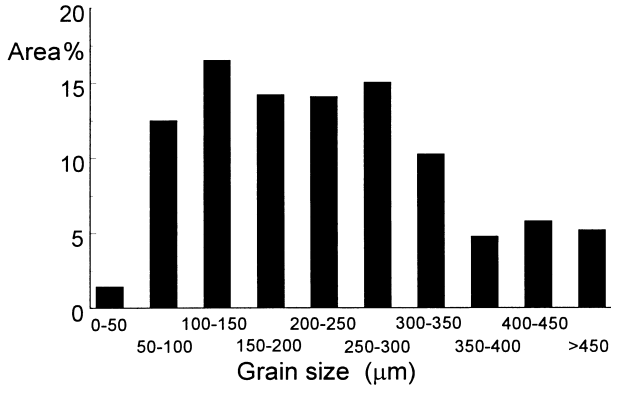

Fig. 1. Grain size distribution of spine.[21]

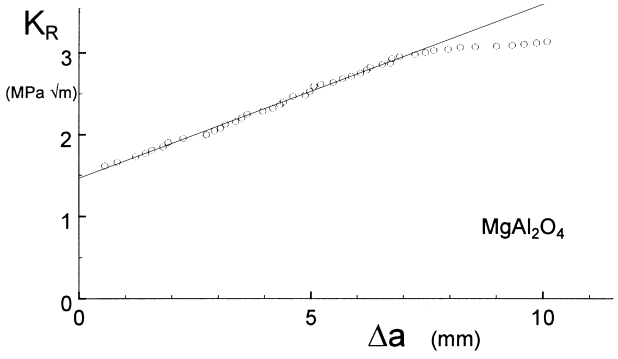

Fig. 3. R-curve for spinel from DCB tests.[21]

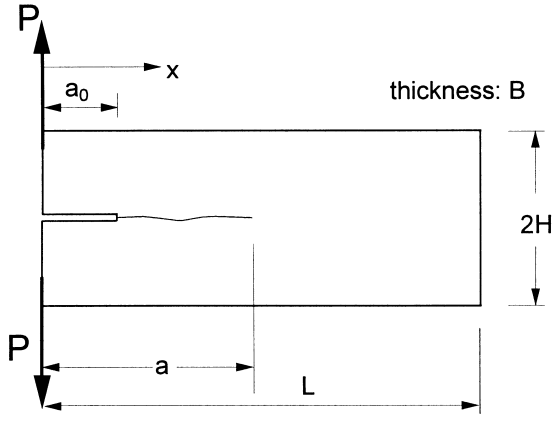

Fig. 2. Geometric data of the DCB-specimen.

$$\sigma(x) = \sigma_{\mathrm{appl}}(x) + \sigma_{\mathrm{br}}(x)\,.$$

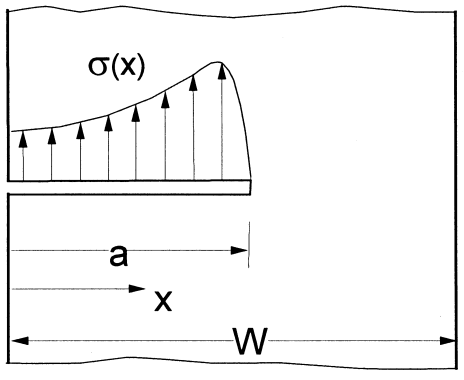

Fig. 4. Crack with arbitary crack face loading $\sigma(\chi)$.

of the component, but is independent of the applied loading. The weight function for the DCB specimen reads as[23]

$$h = \sqrt{\frac{12}{H}}\left[\frac{a-x}{H} + 0.68\right] + \sqrt{\frac{2}{\pi(a-x)}}\exp\left(-\sqrt{12\frac{a-x}{H}}\right), \tag{5}$$

where H is the half height as defined in Fig. 2. The weight function for the DCB specimen used in the experiments is shown in Fig. 5 and the applied stress intensity factor is

$$K_{\text{appl}} = h(0, a)\, P/B. \tag{6}$$

Here $h(0, a)$ is the value of the weight function at location $x = 0$, i.e where the applied forces P act.

The total displacements of the crack surface, δ, can be derived from prior knowledge of the weight function and stress intensity factor for a given stress distribution $\sigma(x)$ as proposed by Rice[24]

$$h(x, a) = \frac{E'}{K_{\text{I}}}\ \frac{\partial\delta(x, a)}{\partial a}. \tag{7}$$

Integration of this formula yields the following expression for δ:

$$\delta(x) = \frac{1}{E'}\int_x^a h(x, a')\, K(a')\, \mathrm{d}a'. \tag{8}$$

If the stress intensity factor $K(a')$ is caused by distributed stresses σ, we have to apply Eq. (4) which results in

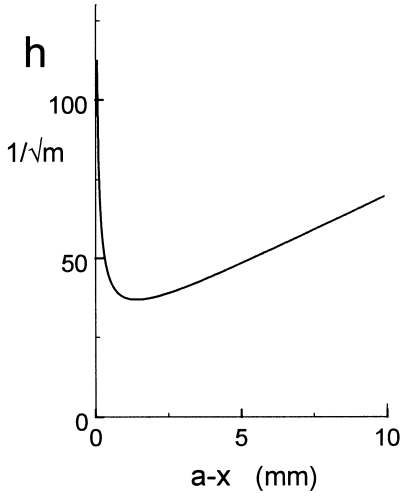

Fig. 5. Weight function for the DCB-specimen used for the experiments.

$$\delta = \frac{1}{E'}\int_x^a h(x, a')\left[\int_0^{a'} h(x', a')\sigma(x')\,\mathrm{d}x'\right]\ \mathrm{d}a', \tag{9}$$

where the displacement has been computed at x, and x' is the location of the stress, σ. Eq. (5) can also be derived from Castigliano's theorem (see Ref. 25).

The stress intensity factors describing the R-curve behavior can be obtained in the following manner:

The total crack opening displacements,

$$\delta = \delta_{\text{appl}} + \delta_{\text{br}}, \tag{10}$$

result from the solution of the integral equation

$$\delta(x) = \frac{1}{E'}\int_x^a h(x, a') \left[\int_0^{a'} h(x', a')[\sigma_{\text{appl}}(x') + \sigma_{\text{br}}(\delta(x'))]\,\mathrm{d}x'\right]\ \mathrm{d}a'. \tag{11}$$

The solution to this equation may be determined by several methods. The simplest one is an iterative approximation. Initially, the applied stress, σ_{appl}, is introduced into the integrand to yield the crack face separation, δ_{appl}. A first approximation for the bridging stresses, σ_{br}, is then obtained by substituting δ_{appl} into the bridging stress law. The bridging stresses obtained are then reintroduced into Eq. (11) and the procedure is repeated until $\delta(x)$ is constant.

The related bridging stress intensity factor is given by

$$K_{\text{br}} = \int_{a_0}^a h(x, a)\,\sigma_{\text{br}}(x)\ \mathrm{d}x, \tag{12}$$

and the applied stress intensity factor K_{appl} as

$$K_{\text{appl}} = \int_0^a h(x, a)\,\sigma_{\text{appl}}(x)\ \mathrm{d}x. \tag{13}$$

Finally, the crack-tip stress intensity factor is given by

$$K_{\text{tip}} = K_{\text{appl}} + K_{\text{br}}. \tag{14}$$

4. Evaluation of the experimental results

Due to the long linear range of the R-curve in Fig. 3, a very simple approach is possible to obtain the bridging stresses. From Eqs. (2), (5) and (12) we can conclude that for crack extensions within the straight part of the R-curve, the distribution of the bridging stress must be reciprocal to the weight function, i.e.

$$\int_{a_0}^a h(x, a)\,\sigma_{\text{br}}\,dx = C(a - a_0) \Longleftrightarrow h(x, a)\,\sigma_{\text{br}} = C \Longleftrightarrow \sigma_{\text{br}} = C/h \tag{15}$$

The resulting bridging stresses, plotted in Fig. 6 as a function of the coordinate x, are determined by combining Eqs. (5) and (15).

The corresponding crack opening displacements were computed by introducing K_{app}, from Eq. (6), into Eq. (8) and σ_{br} from Eq. (15) into Eq. (9). The displacements, δ_{appl} and δ_{br}, are shown in Fig. 7 together with the total crack profile, δ, obtained from Eq. (12).

In this context, it should be noted that in the literature, often only near-tip solutions for the crack opening displacement are used for δ. It may be concluded from Fig. 7, that such approximations are not appropriate for accurate displacement calculations. This will be shown in more detail in the Appendix.

The evaluation of bridging stresses from R-curve data is based on the solution of Eqs. (11)–(14). The numerical strategy consists of the following steps:

1. For small displacements (corresponding to crack extensions where $\Delta a \leqslant 5$ mm) the bridging relation results from Eq. (15) with the displacements computed by Eq. (9). The result is shown in Fig. 8a.
2. For larger displacements, the $\sigma_{br}(\delta)$ function is represented by the stress values at the sampling points δ_1 and δ_2, which are interpolated by cubic splines (Fig. 8b).
3. The bridging stresses (see Fig. 8b) in the range $\delta \leqslant 4$ μm were computed for chosen values of $\sigma_{br}(\delta_1)$ and $\sigma_{br}(\delta_2)$. The integral equation was solved and the crack profile and the bridging stress distribution were obtained. From Eq. (12) the associated bridging stress intensity factor, K_{br}, was calculated and using Eq. (1) the R-curve values, K_R, were obtained for a number of selected Δa. The computed K_R values were then compared to the experimental data. The bridging stress values at δ_1 and δ_2 were changed systematically by use of the Harwell computer subroutine, VA02AD, until minimum deviations between the computed and measured K_R were found. The corresponding bridging stresses at δ_1 and δ_2 then establish the bridging stress function, $\sigma_{br}(\delta)$, for larger crack opening displacements (Fig. 8c). Fig. 9 gives a comparison of the computed K_R-values with the measured ones.

It should be mentioned that the bridging stresses for any R-curve can be determined using this technique. The initial part of the bridging stress function may also be represented by cubic splines. Unfortunately, the number of sampling points must be increased for this purpose, which drastically increases the numerical effort.

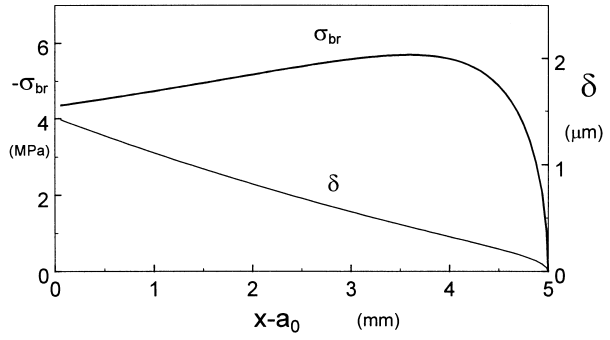

Fig. 6. Bridging stress distribution along the crack for $a-a_0=5$ mm.

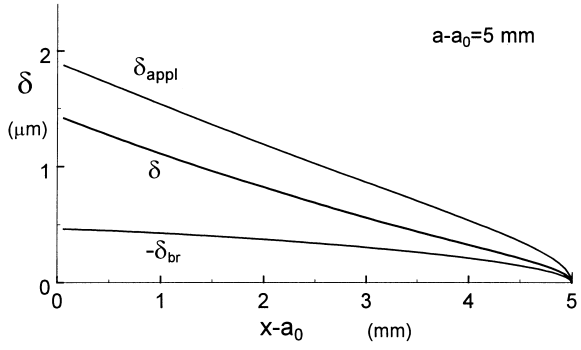

Fig. 7. Total crack profile δ composed by the applied and the bridging displacements.

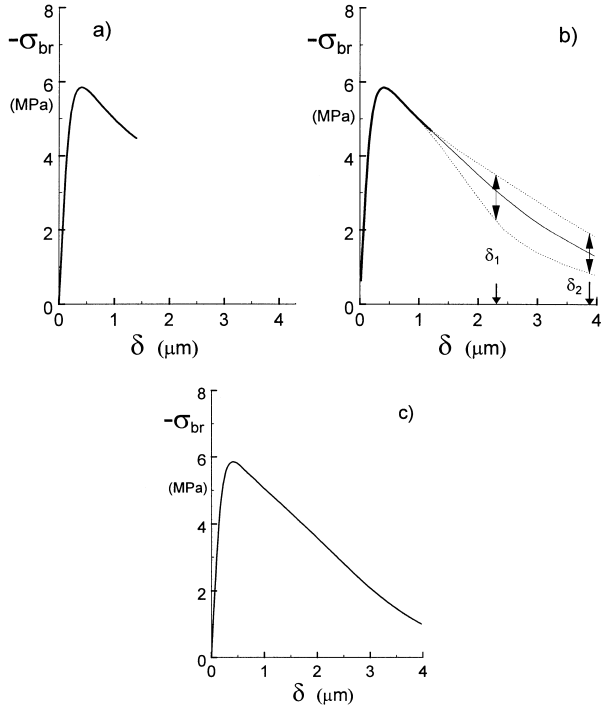

Fig. 8. Determination of the bridging relation: (a) solution for small displacements from linear part of the R-curve, (b) representation of relation for large displacements by cubic splines (two sampling points), (c) final result.

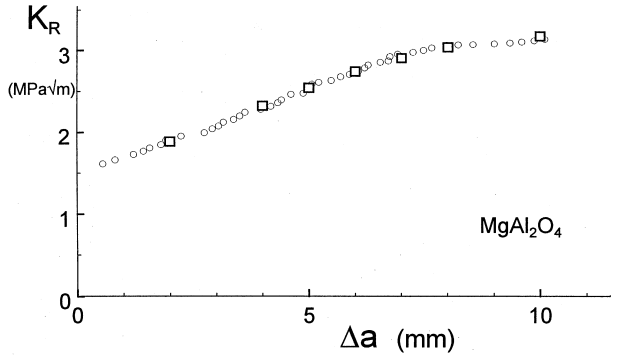

Fig. 9. R-curve data computed from the bringing stress relation Fig. 8c (squares) compared with the measurements (circles).

5. Summary and conclusions

A procedure is proposed which allows for the determination of the bridging stress function from a given R-curve. An application of the method is illustrated for a coarse-grained spinel exhibiting an extended linear R-curve behavior. For this special case, an analytical solution for the small displacement behavior is applied. For the treatment of large displacements the bridging function in the form of $\sigma_{\mathrm{br}}=f(\delta)$ was described by (a priori unknown) stress values at two sampling points, δ_1 and δ_2, which were interpolated by cubic splines. Application of a fitting procedure allowed the unknown stress values to be determined. As a result, an initially increasing bridging stress is found which decreases at larger crack opening displacements.

Appendix. Accuracy of approximate crack opening displacement fields

The correct displacements $\delta(x)$ for any prescribed stress distribution can be obtained by evaluating Eq. (9). Nevertheless, one will often find approximations which are neither influenced by the shape of the stress distribution nor by the geometry of the test specimen. Such estimations, describing the near-tip displacements, are not appropriate to evaluate the bridging stresses. The poor agreement of such attempts with the exact solution will be demonstrated here, for different degrees of approximation. The basis of each estimation will be Eq. (8).

As a consequence of the Williams stress function [26] for edge-cracked specimens, the weight function may be expressed as

$$h = h_{\mathrm{tip}} + O(a-x)^{1/2}, \quad h_{\mathrm{tip}} = \sqrt{\frac{2}{\pi(a-x)}} \tag{A1}$$

where h_{tip} defines the singular near tip term.

Since the singular term must be present in all weight functions independent of the special specimen size and shape, let us first replace the correct weight function occurring in Eq. (8) by the near-tip term, i.e.

$$\delta(x) \cong \frac{1}{E'}\int_x^a \sqrt{\frac{2}{\pi(a-x)}}\,K(a')\,\mathrm{d}a'. \tag{A2}$$

The main contribution to the integral arises for $a'\to a$. Therefore, let us replace $K(a')=K(a)$ in Eq. (A2) with the resulting near-tip solution

$$\delta_0 = \sqrt{\frac{8}{\pi}}\,\frac{K_I}{E'}\sqrt{a-x} \tag{A3}$$

which is well-known in fracture mechanics.[27] Another often used near-tip solution has been proposed by Barenblatt[28] which reads in our coordinate system

$$\delta_1 = \sqrt{\frac{2}{\pi}}\,\frac{K_{\mathrm{tip}}}{E'}\sqrt{a-x} + \frac{4}{\pi E'}\int_{a_0}^{a}\sigma_{\mathrm{br}} \left[\sqrt{\frac{a-x}{a-x'}} - \tfrac{1}{2}\ln\left(\left|\frac{\sqrt{a-x'}+\sqrt{a-x}}{\sqrt{a-x'}-\sqrt{a-x}}\right|\right)\right] dx' \tag{A4}$$

For a further improvement of the near-tip solutions let us make use of the usual representation of stress intensity factors,

$$K = \sigma^* Y\sqrt{a}, \tag{A5}$$

with a characteristic stress σ^* and a geometric function Y depending on specimen geometry, crack size and special loading situation. Eq. (A5) gives rise to an approximation of $K(a')$ for $a'\to a$ of

$$\frac{K(a')}{K(a)} = \sqrt{\frac{a'}{a}}, \tag{A6}$$

which may be used in Eq. (8). Together with use of the correct weight function we obtain

$$\delta_2 \cong \frac{K}{\sqrt{a}E'}\int_x^a h(x,a')\sqrt{a'}\,\mathrm{d}a' \tag{A7}$$

As an example of application let us use the stress distribution given by Eq. (15). For these stresses the displacements were computed with Eq. (9) for a crack propagation of $\Delta a=5$ mm and $K_{\mathrm{tip}}=K_{\mathrm{I0}}$.

The approximations δ_0, δ_1, and δ_2 are compared in Fig. A1 with the result δ from Eq. (9). It can be seen that the approximations δ_0 and δ_1 show large deviations from the true crack profile. In the case of approximation δ_2 the deviations are relatively small. In Fig. A1b

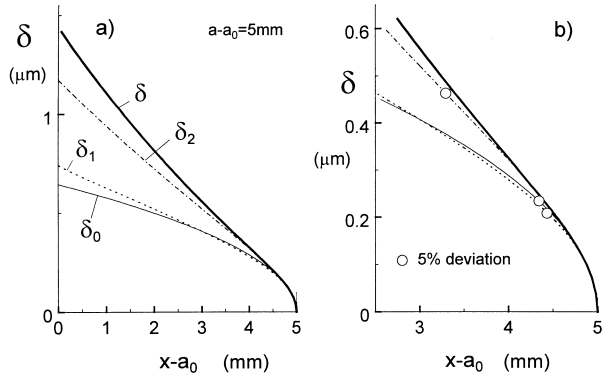

Fig. A1. Comparison of approximate crack opening displacements with the exact crack profile (solid curve).

the circles represent those points where the approximations deviate by 5% from the correct result. Whereas this error margin is reached for approximations δ_0 and δ_1 at about 0.6 mm distance from the crack tip, this distance increases in case of δ_2 significantly to 1.7 mm.

As the consequence of the considerations outlined previously, it is recommended to compute the correct displacements and to avoid the application of near-tip displacement fields δ_0 and δ_1 to the whole crack.

References

1. Knehans, R. and Steinbrech, R., Memory effect of crack resistance during slow crack growth in notched Al_2O_3 bend specimens. *J. Mater. Sci. Lett*., 1982, **1**, 327–329.
2. Steinbrech, R., Knehans, R. and Schaarwächter, W., Increase of crack resistance during slow crack growth in Al_2O_3 bend specimens. *J. Mater. Sci*., 1983, **18**, 265–270.
3. Frei, H. and Grathwohl, G., The fracture resistance of high performance ceramics by in situ experiments in the SEM. *Beitr. Elektronenmikroskop. Direktabb. Oberfl*, 1989, **22**, 71–78.
4. Lathabai, S., Rödel, J. and Lawn, B. R., Cyclic fatigue from frictional degradation at bridging grains in alumina. *J. Am. Ceram. Soc*., 1991, **74**, 1340–1348.
5. Steinbrech, R. and Schmenkel, O., Crack resistance curves for surface cracks in alumina. *Comm. J. Am. Ceram. Soc*., 1988, **71**, C271–C273.
6. Fett, T. and Munz, D., Evaluation of R-curve effects in ceramics. *J. Mater. Sci*., 1993, **28**, 742–752.
7. Munz, D. and Fett, T., *Ceramics, Failure, Material Selection, Design*. Springer-Verlag, März, 1999.
8. Rödel, J., Kelly, J. F. and Lawn, B. R., In situ measurements of bridged crack interfaces in the scanning electron microscope. *J. Am. Ceram. Soc*., 1990, **73**, 3313–3318.
9. Yu, C. T. and Kobayashi, A. S., Fracture process zone in SiC_W/Al_2O_3. *Ceram. Eng. Sci. Proc*, 1993, **14**, 273–283.
10. Fett, T., Munz, D., Yu, C. T. and Kobayashi, A. S., Determination of bridging stresses in reinforced Al_2O_3. *J. Am. Ceram. Soc*., 1994, **77**, 3267–3269.
11. Fett, T., Munz, D., Seidel, J., Stech, M. and Rödel, J., Correlation between long and short crack R-curves in alumina using the crack opening displacement and fracture mechanical weight function approach. *J. Am. Ceram. Soc*., 1996, **79**, 1189–1196.
12. Fett, T., Munz, D., Thun, G. and Bahr, H. A., Evaluation of bridging parameters in Al_2O_3 from R-curves by use of the fracture mechanical weight function. *J. Am. Ceram. Soc*., 1995, **78**, 949–951.
13. Fett, T., Contributions to the R-curve behaviour of ceramic materials, KfK-Report 5291, Kernforschungszentrum Karlsruhe, 1994.
14. Fett, T., Determination of bridging stresses and R-curves from load-displacement curves. *Engng. Fract. Mech*, 1995, **52**, 803–810.
15. Erdogan, Z. and Joseph, P. F., Toughening of ceramics through crack bridging by ductile particles. *J. Am. Ceram. Soc*., 1989, **72**, 262–270.
16. Sarrafi-Nour, G. R., Coyle, T. W. Application of the weight-function method to study the R-curve behavior of ceramics using chevron-notched specimens. *J. Am. Ceram. Soc*., in press.
17. Sarrafi-Nour, G.R., Temperature dependence of crack wake bridging stresses in silicon carbide-reinforced alumina composite. PhD thesis, University of Toronto, 1999.
18. Hay, J. C. and White, K. W., Grain-bridging mechanisms in monolithic alumina. *J. Am. Ceram. Soc*., 1993, **76**, 1849–1854.
19. White, K. W. and Hay, J. C., The effect of thermoelastic anisotropy on the R-curve behavior of monolithic alumina. *J. Am. Ceram. Soc*., 1994, **77**, 2283–2288.
20. Hay, J. C. and White, K. W., Grain boundary phases and wake zone characterization in monolithic alumina. *J. Am. Ceram. Soc*., 1995, **78**, 1025–1032.
21. Olasz, L., Ortiz-Longo, C.R., and White, K.W., Characterization of microstructure- mechanical behavior relationships of crack wake zone bridging elements in monolithic ceramics under cyclic loading, *J. Am. Ceram. Soc*., submitted.
22. Bueckner, H., A novel principle for the computation of stress intensity factors. *Zeitschrift für Angewandte Mathematik und Mechanik ZAMM*, 1979, **50**, 529–546.
23. Fett, T. and Munz, D., *Stress Intensity Factors and Weight Functions, Computational Mechanics Publications*. Computational Mechanics Publications, Southampton, UK, 1997.
24. Rice, J. R., Some remarks on elastic crack-tip stress fields. *Int. J. Solids Struct*, 1972, **8**, 751–758.
25. Cox, B. N. and Marshall, D. B., Stable and unstable solutions for bridged cracks in various specimens. *Acta Metall*, 1991, **39**, 579–589.
26. Williams, M. L., On the stress distribution at the base of a stationary crack. *J. Appl. Mech*, 1957, **24**, 109–114.
27. Irwin, G.R. *Fracture, Handbuch der Physik*, Vol. VI. Springer, Berlin, 1958.
28. Barenblatt, G. I., The mathematical theory of equilibrium cracks in brittle fracture. *Adv. Appl. Mech*., 1962, **7**, 55.